A Review of the Behavior of Fuel Drops in a Fuel Spray in the Context of Biofuels

Riho Kägo, Risto Ilves*, Arne Küüt, Jüri Olt

Estonian University of Life Sciences, Institute of Technology, Kreutzwaldi 56, Tartu, 51006, Estonia

Abstract

In addition to gasoline and diesel fuel, the biofuels HVO and FAME have been taken into wide use during the last decades. The properties of gasoline and diesel fuel and their effect on the combustion process have been studied for a long time, but studies on HVO and FAME are still are very much work-in-progress. Existing studies show that the use of biodiesels reduces the level of several exhaust gas emissions (like soot) in engine exhaust gases. At the same time, the reasons for the reduction of emission compounds remain unclear. The motivation behind determining drop size and behavior is to aid assessment of the quality of the air-fuel mixture with a view to explaining the reduction in soot emission when biodiesels are used. The aim of this review paper is to provide an overview of the behavior of fuel drops and their size in fuel injectors when using different biofuels by giving a theoretical background based on literature, on the basis of which the calculations give an opportunity to evaluate experimental results of the behavior of different biofuels in the fuel spray. This study compares four different fuel types according to the WAVE-RT model. In addition, the collision mechanisms of drops (reflexive and stretching separation) are presented and these shall be compared for the fuel types. The results show that during the use of biofuels, the drop size is somewhat larger compared to diesel fuel.

Keywords: biodiesel, fuel drop size, FAME, HVO, diesel engine

1. Introduction

The use of biofuels is growing in the world. An EU directive prescribes that by 2020 biofuels must make up 10% of the energy used in the transport sector [1]. The Paris Agreement aims to further increase the share of biofuels in the transport sector. Several studies have been performed on the use of biofuels in internal combustion engines. The main focus has been on the effects of biofuels on engine exhaust gases, work surfaces, fuel preservation, blending with fossil fuels etc. The results show that when, for example, biodiesel (for example, FAME or RME) is used as engine fuel, the level of soot in exhaust gases decreases. At this point, the decrease in the level of soot in exhaust gases is explained by more efficient combustion, as biodiesel contains oxygen [2–58].

At the same time, when HVO is used, the level of soot in engine exhaust gas is also reduced [59, 60]. Therefore, the oxygen content in the fuel cannot be used as the actual reason for explaining the reduction in soot levels.

In order to provide a better overview, a theoretical analysis of the injection of biofuels into engines must be performed. There is currently no summary available on injection mechanisms in respect of biofuels, the behavior of fuel drops in fuel

sprays and the distinctive features of the behavior of biofuels compared to regular fuels. As drop size is an important factor in determining fuel evaporation and combustion in the engine cylinder, this analysis may provide some explanations about the formation of biofuel sprays and about the characteristics of the combustion of biofuels.

Therefore, the aim of the article is to provide an overview of the behavior of fuel drops and their size in fuel sprays when various biodiesels (hereinafter "biofuels") are used. The motivation behind determining drop size and behavior is to aid assessment of the quality of the air-fuel mixture in order to explain the reduction in soot emission when biofuels are used. The theoretical part is based on the fuel drop formation models, which are used to perform the calculations to describe the behavior of various biofuels in the fuel spray. The article describes the formation of fuel drops, points out their impact parameters and analyzes the behavior of biofuel drops in the fuel spray.

The main theoretical assumptions on which this paper is based:

1. Sprayed fuel drops are considered as (symmetrical) physical bodies, with the ability to bounce, coalesce and separate from each other [61–65].
2. The ability to bounce, coalesce and separate from each

---

other is dependent on intrinsic and environmental physical properties (pressure, temperature, etc.) [66–68].

3. The spraying process is considered as a two-phase event: primary breakout of the fluid and the formation of droplets. Several theories describe this event: WAVE-RT, WAVE-TAB, WAVE-KH, etc., each with a respective mathematical interpretation [69–71].

The detailed mathematical background will be discussed in Sections 3 (Parameters describing fuel drop formation and collision), 4 (Fuel drop size after leaving the injector), 5 (Hybrid breakout model) and 6 (Mathematical representation of reflexive and stretching separation).

The topic of the article is related to the scope of the Journal of the Power and Technologies through the theme of renewable energy. The article provides an overview of the behavior of biofuel drops in the spray and supplements the database of the journal with explanations of biofuel spray issues.

2. Problem description

When biofuels, for example, FAME, are used as fuel in a diesel engine, generally the soot level in the exhaust gas decreases but there are increases in the number of soot particles and the emission of carbon dioxide and nitrogen compounds in the exhaust gas. The increased level of nitrogen compounds and CO_2 and the reduction in soot level is caused by the more efficient combustion of biofuels (HVO, FAME) in the engine. The more efficient combustion has been explained by the biofuel's oxygen content, which improves the combustion of the fuel. In addition, sources discuss in great detail the carbon-hydrogen ratio in the fuel [20, 31, 32, 39, 58–60].

Unfortunately, the reasons given in these scientific sources are not in conformity with generally known theories, because, for example, the diesel engine always works with a lean mixture, where the value of the air-fuel equivalent ratio is usually greater than 1.25. For turbo engines, this value is greater than ~4 [72]. Therefore, the cylinder of a diesel engine contains a theoretically sufficient amount of oxygen for the complete combustion of fuel. In addition, the engine tests of HVO fuel run contrary to the FAME results. HVO fuel does not contain oxygen, but the soot level in the emission gas is reduced. It is also questionable how the carbon-hydrogen ratio affects the emission gas. If we presume that for the engine to work on the same load, the same amount of energy must be added and this is derived from the fuel carbon-hydrogen ratio; then the fuel added to the engine always has the same magnitude of carbon-hydrogen atoms. Further, the test results show a contradiction in fuel properties and fuel behavior during injection.

Table 1 compares the physical properties of diesel fuel (DF), HVO and FAME obtained by testing according to the EN-590 standard. The properties of gasoline are obtained from source [73]. To avoid possibly misleading fuel properties as listed in sources, the data listed in the table above

was obtained by testing. In the table, gasoline is given as reference fuel for comparing low viscosity fuels with high viscosity fuel. Table 1 shows, for example, that HVO and FAME have greater viscosity than diesel fuel. According to general knowledge, as the viscosity of the fuel increases, so does the size of fuel drops in the fuel spray, which also increases the combustion time. The longer combustion time prevents large fuel drops from combusting completely, which increases the level of soot in the emission gas. In our case, this is in contradiction with the results given in previous studies. When comparing fuel weight fractions, HVO fuel contains lighter fractions compared to diesel fuel. It can be said about FAME fuel that this fuel contains significantly more heavy fractions compared to diesel fuel (when the temperatures of the evaporated parts (10%–90%) of fuel are compared). Likewise, the heavy fractions of fuel need more time for combustion. Therefore, the soot level in the emission gas of FAME fuel must be at least of the same magnitude as diesel fuel. The following chapters provide an overview of the behavior of fuel drops in the fuel spray and describe the effect of the properties of biofuels on fuel drop size.

The method of literature overview and the modeling of fuel drop behavior in the spray were chosen with this issue in mind. Theoretical calculations give an opportunity to evaluate experimental results of the behavior of different biofuels in the fuel spray and explain the reasons for the problem.

3. Parameters describing fuel drop formation and collision

When fuel is sprayed, the fuel spray breaks down into drops. As the fuel drops move in the fuel spray, the drops are broken down by air resistance and collisions take place between drops, which changes the drop size dc (Sauter Mean Diameter, *SMD* -d_{32}).

Three dimensionless parameters are used to model the decomposition of fuel drops:

Weber number *We*

$$We = \frac{\rho \cdot |v_1 + v_2|^2 \cdot (D_1 - D_2)}{\sigma} \tag{1}$$

where ρ is the fluid's density (kg/m^3), *v1* and *v2* are the respective speeds of smaller and bigger drops (m/s), D_1 and D_2 are the respective diameters of the drops (m) and σ is the fluid's surface tension factor (N/m).

Impact parameter *B*

$$B = \frac{2b}{(D_1 + D_2)} \tag{2}$$

where *b* is the distance from the center of one drop to the relative velocity vector placed to the center of the other drop (m). $B = 0$ corresponds to the frontal impact of the drops and $B = 1$ corresponds to the situation in which the drops graze each other (Fig. 1).

Drop size ratio γ

Table 1: Properties of diesel fuel and biofuels used in diesel engines

| Parameter	Unit	Method	GAS	DF	HVO	FAME
Density (15℃)	kg/m³	EN ISO 12185	703	837	781	885
Fractional distillation						
Initial boiling point (IBP)	℃			150	170	280
BP 10%	℃			205	252	330
BP 20%	℃			222	265	332
BP 30%	℃			236	270	333
BP 50%	℃			260	276	334
BP 60%	℃			275	278	334
BP 70%	℃			292	280	334
BP 80%	℃			310	283	334
BP 90%	℃			332	288	334
BP 95%	℃			346	292	334
Evaporated at temperature (180℃)	vol%			4	3	0
Evaporated at temperature (250℃)	vol%			42.5	10.0	0
Evaporated at temperature (350℃)	vol%			96	-	-
Final boiling point (FBP)	℃			352	305	334
Recovery	vol%			98.0	98.5	99.0
Residue	vol %			1.8	1.5	1.0
Loss	vol %			0.2	0	0
Kinematic viscosity (40℃)	mm2/s	EN ISO 3104	1.223	2.827	3.039	4.573
Dynamic viscosity (40℃)	mPa·s	EN ISO 3104	0.86	2.32	2.30	3.93
Sulfur content	mg/kg	EN ISO 20846		6.7	0.5	7.3
Kinematic viscosity (90℃)	mm²/s		0.53	1.31	1.36	1.98
Dynamic viscosity (90℃)	mPa·s		0.038	0.107	0.104	0.171
Surface tension (90℃)	N/m		0.018	0.020	0.023	0.021
Density (90℃)	kg/m³		709	820	762	867
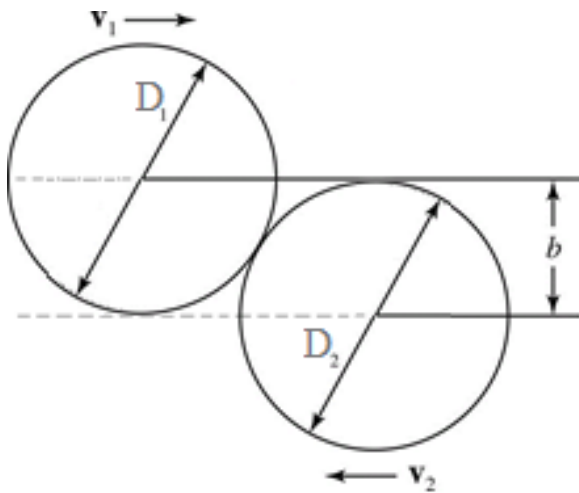
Figure 1: An explanation of impact parameter B , where b is the distance from the center of one drop to the relative velocity vector placed to the center of the other drop (m), $v1$ and $v2$ are the respective speeds of smaller and bigger drops (m/s) and D_1 and D_2 are the respective diameters of the drops (m).

$$\gamma = \frac{D_2}{D_1} \qquad (3)$$

$$\Delta = \frac{D_1}{D_2} \qquad (4)$$

Depending on these three parameters, the collision of two drops may have five possible results [61–63, 74–80]:

1. slow coalescence,
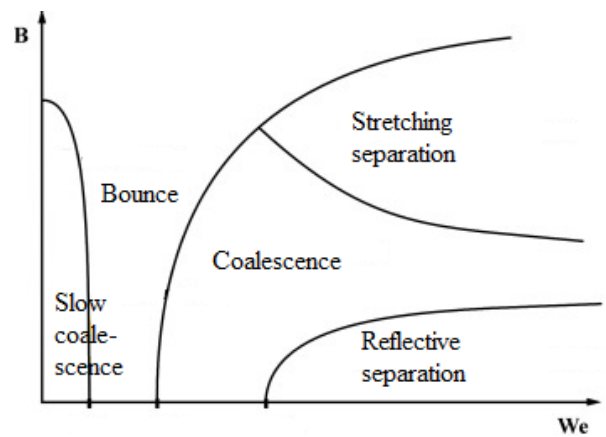2. bounce,
3. coalescence,
4. reflexive separation,

Figure 2: Drop-drop collision mechanisms [81]

5. stretching separation.

The possible results of collision of drops are given in Fig. 2 [81].

In the case of reflexive and stretching separation, satellite drops are formed in addition to daughter drops. The mechanism of satellite drop formation is described by Plateau-Rayleigh instability [82, 83]. The diameter $d$sat and number N sat of satellite drops can be modelled using the Munnannur-Reitz model [84], whereby both of these depend on the Weber number. Fig. 3 depicts the possibilities $B = f(We)$ as a diagram [66].

Situation $B = 0$ corresponds to the frontal impact of two drops. The colliding drop size ratio in this diagram is $\gamma = 1$, which corresponds to the situation in which the colliding drops have equal diameters. If γ is increased to values of 100 and more, then cohesion forces increase the probability of coalescence of the drops. If the ambient pressure p is
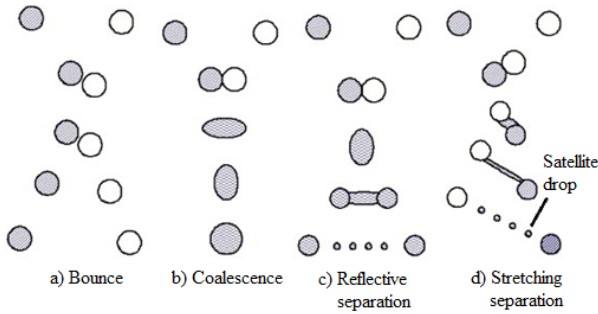
Figure 3: Possible results of the collision of two drops at ambient temperature $T = 300$ K and pressure $p = 1$ atm [66].

Table 2: Values of *SMD* from chosen authors

Author	[66]	[66]	[87]
Environment	Nitrogen	Nitrogen	-
Pressure p (atm)	1.0	2.4	-
Temperature T (K)	300	300	1000
Environment (gas) density ρ_g (kg/m$_3$)	-	-	14.8
Spray diameter d$_0$ (μm)	246	246	-
Fuel	Tertadecane (DF)	Tertadecane (DF)	-
Fuel density ρ_l (kg/m³)	763	763	-
Surface tension factor σ (N/m)	2.18·10^{-2}	2.18·10^{-2}	-
SMD (μm)	9.5	4.1	0.84

increased, then the slow coalescence area disappears, as it becomes harder during collision to squeeze out the gas (air) between the drops.

From the point of view of biofuels, it is important to note that the size of drops during spraying depends mostly on their physical and chemical properties, density, surface tension, viscosity. These properties of fuels are the main causes why different fuels form different properties of air-fuel mixtures in the engine cylinder and why the combustion properties are different. Fuel drop size is crucial during combustion of the air-fuel mixture, as it directly affects combustion efficiency and engine exhaust gas.

4. Fuel drop size after leaving the injector

The size of the fuel drop after leaving the injector can be expressed as follows [85]:

$$d_c = \frac{2\pi B_d \sigma \lambda_m}{\rho_a U_T^2} \qquad (5)$$

where B_d is a parameter that depends on the injector nozzle's geometry. In previous works [86] the value of B_d was chosen $B_d = 0.62$, σ − fluid's (gasoline, DF, HVO, FAME) surface tension factor (N/m), λ_m − fluid's Taylor viscosity parameter, ρ_a − density of outer or gas environment (kg/m³), U_T − velocity of the fastest unstable wave of the spray (m/s), whereby U_T is in linear correlation with the initial velocity of the injected spray. Here $U_T = 0.25\, U_0$, where U_0 is the initial velocity of the spray (m/s).

It is possible to obtain the mean diameter of drops leaving the injector or Sauter mean diameter (*SMD*) by using equation (5) and data listed in sources [66, 87]. Table 2 presents some illustrative *SMD* values according to various authors.

Here it should be pointed out that in addition to *SMD*, other parameters are used to describe the drops, for example, *d10*, *d20*, *d30*, *d43* (Herdan Mean Diameter or *HMD*), etc. [88, 89]. *SMD* is related to the volume-area ratio and describes the mean size of fuel drops in the fuel spray. Therefore, this parameter is used in most of the equations related to the formation of air-fuel mixtures and the combustion of fuel sprays and air-fuel mixtures.

Sources [90–92] point out several methods for determining the *SMD* of drops leaving the injector. The following equations are common for diesel engines:

$$SMD = 4,12d\text{Re}^{0,12}\text{We}^{-0,54}\left(\frac{\mu_f}{\mu_g}\right)^{0,54} \qquad (6)$$

$$SMD = 0,38d\text{Re}^{0,25}\text{We}^{-0,32}\left(\frac{\mu_f}{\mu_g}\right)^{0,37}\left(\frac{\rho_f}{\rho_g}\right)^{-0,47} \qquad (7)$$

$$SMD = 8,7\,(\text{Re}_l\text{We}_l)^{-0,28}\,d_0 \qquad (8)$$

where *Re* and *We* are respective Reynolds and Weber numbers, μ − fuel dynamic viscosity (Pa·s), ρ − density (kg/m³), d_0 is the diameter of injector's opening (m). Index "*f*" denotes "fluid" and "*g*" denotes "gas".

In addition to the abovementioned sources there are other authors [81, 93–96], who give a theoretical and experimental assessment of *SMD* in their work. Results are mostly given as functions of time and distance $SMD = f(t)$ and $SMD = f(x)$ as the sprayed fuel drops constantly change their size (coalescence, reflexive separation and stretching separation with satellite drops). The *SMD* values of these works remain in the range of 40–100 μm.

5. Hybrid breakout model (WAVE)

The size of fuel drops changes continuously after leaving the injector, depending on ambient temperature, drop velocity, distance etc. The size and change can be described using WAVE (hybrid breakout) models. WAVE models can be used to describe breakout of various biofuels (HVO, FAME) and the size of their drops in fuel spray.

The breakout of fuel spray that has left the injector takes place in two stages. First, the fuel is sprayed into drops (primary breakout). Then, the drops break out once again due to aerodynamic forces (secondary breakout) [97–101]. This dual-stage process can be described according to hybrid breakout model of drops (Fig. 4).

There are several hybrid breakout models: WAVE-RT [69, 70, 102–105], WAVE-TAB [71, 106–108], WAVE-DDB [109, 110], WAVE-ACT [111], etc. Various models were compared in overview article [112]. The relations used in this study are given according to the WAVE-RT model, which has
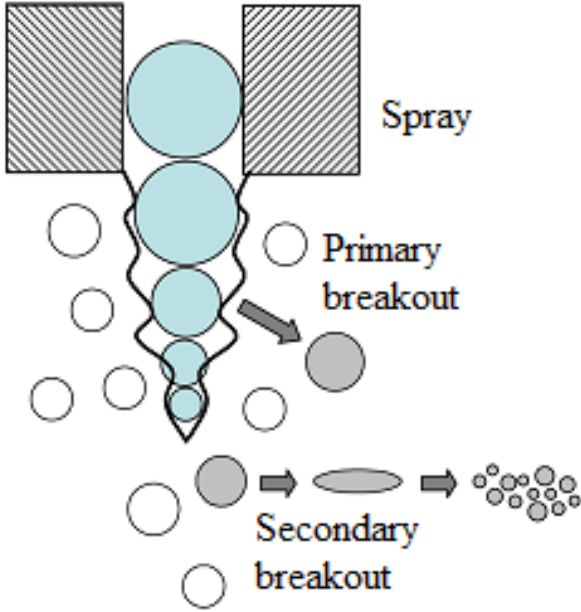
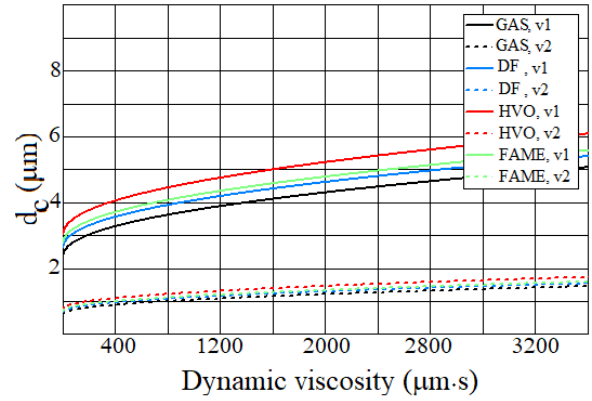Figure 4: Schematic drawing of hybrid breakout model [81]

Figure 5: Dependency between the diameter dc of the drop leaving the injector and fluid's dynamic viscosity μ at two different velocities v of the spray (v_1 = 200 m/s, v_2 = 400 m/s), for four different fuel types. The x-axis value range 0-3600 μPa·s corresponds to typical viscosities of fuels at temperatures 40℃ and 90℃ (Table 1)

been most widely used in research. According to the original WAVE model, the surface of the fluid leaving the injector develops Kelvin-Helmholtz instability, which leads to the emerging of sinusoidal surface waves. These waves lead to the separation of the unstable part of fluid from the spray, which in turn leads to the generation of drops. According to the WAVE model [71, 109], drop growth speed Ω_{KH} and corresponding wavelength Λ_{KH} are represented as follows:

$$\frac{\Lambda_{\mathrm{KH}}}{r} = 9,02 \frac{\left(1 + 0,45Z^{0,5}\right)\left(1 + 0,4T^{0,7}\right)}{\left(1 + 0.87\mathrm{We}_g^{1,67}\right)^{0,6}} \qquad (9)$$

$$\Omega_{\mathrm{KH}}\left(\frac{\rho_f r^3}{\sigma_f}\right)^{0.5} = \frac{(0,34 + 0,38\mathrm{We}_g^{1,5})}{(1 + Z)(1 + 1,4T^{0,6})} \qquad (10)$$

The relations (9) and (10) contain members which are expressed as follows:

$$d_c = 2B_0\Lambda_{\mathrm{KH}} \qquad (11)$$

$$\tau_{\mathrm{KH}} = \frac{3,726B_1 r}{\Omega_{\mathrm{KH}}\Lambda_{\mathrm{KH}}} \qquad (12)$$

where We and Re are the Weber number and Reynolds number. While the Weber number determines the nature of drops after the possible coalescence of drops, then the Reynolds number characterizes the distribution of drops in a gas environment.

$$Z = \frac{\sqrt{\mathrm{We}_f}}{\mathrm{Re}_f} \qquad (13)$$

$$T = Z\sqrt{\mathrm{We}_g} \qquad (14)$$

$$\mathrm{Re}_f = \frac{\rho_f \mathsf{v} r}{\mu_f} \qquad (15)$$

where ρ_f and ρ_g are the densities of fluid and gas (kg/m³); v – fluid velocity (m/s). In this context, the value of v can be considered equal to velocity of the spray leaving the injector, r – radius of fluid spray leaving the injector (m), μ_f – dynamic viscosity of fluid (Pa·s), σ_f and σ_g – surface tension of fluid and gas (N/m).

The physical and chemical properties of the fuel affect the fuel drop size in the fuel spray. Thus, their influence is described in detail in the following Fig. 5–8. In this research, the range of variated parameters is chosen accordingly to describe the diesel engine work mode. The values of the fuel parameters, by example dynamic viscosity μ_f, density etc. are used based on the condition of the engine.

The following relations are for finding the diameter dc of the drop leaving the injector's spray and drop breakout time τ_{KH} [71, 109]:

$$\mathrm{We}_f = \frac{\rho_f v^2 r}{\sigma_f} \qquad (16)$$

$$\mathrm{We}_g = \frac{\rho_g v^2 r}{\sigma_f} \qquad (17)$$

where B_0 and B_1 are empirical constants with values B_0 = 4.5 and B_1 = 40. Various sources [71, 113, 114] give different values to the constants B_0 and B_1. The values of B_1 are usually within the range 1-60 depending on the characteristics of the injector.

Equation (11) contains the member Λ_{KH}, which contains the fluid's dynamic viscosity μ_f. Therefore, it is possible to represent graphically the dependency dc of the drop leaving the injector and fluid's dynamic viscosity μ_f for various fuels (Fig. 5). The diagrams of Fig. 5 presume that the surface tension and density of fuel does not change. The density of
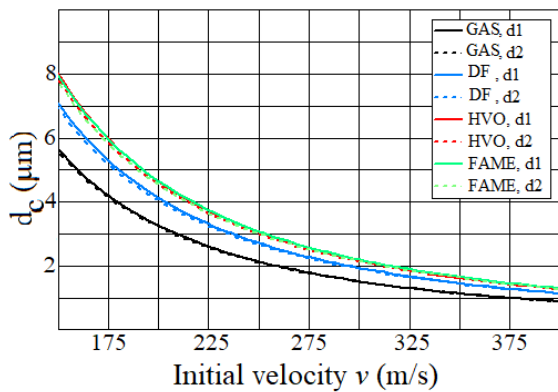
Figure 6: The dependency between the diameter dc of the drop leaving the injector and fluid's initial velocity v in the case of two different diameters d of injector's opening ($d_2 = 100 \mu m$, $d_2 = 300\ \mu m$) in the case of four different fuel types. The x-axis value range 150-400 m/s corresponds to typical velocities of fuel drops in engine practice

Figure 7: Dependency between diameter dc of the drop leaving the injector and injector's diameter d at two spray velocities v ($v1$ = 200 m/s, $v2$ = 400 m/s) with four different fuel types. The x-axis value range 100-300 μm corresponds to typical fuel injector diameters

the gas environment is 17kg/m^3, injector's opening's diameter 100 μm. According to sources [115–121], the physical parameters of the fuels correspond to the temperature 90 °C.

Fig. 5 shows that as the dynamic viscosity increases, the drop size in the air-fuel mixture also increases. An important factor impacting drop size is the velocity of the fuel spray. The higher the velocity of the fuel spray, the smaller the diameter of the drop. Dynamic viscosity has a bigger effect on the change of fuel drop size in the case of lower velocity fuel spray. For example, the change of fuel drop size (any fuel) at the velocity of 400 m/s is smaller than at 200 m/s. Likewise, the physical and chemical properties of fuels have an effect on drop size mostly at lower velocity spray v_1= 200 m/s. When we compare the fuel spray of gasoline and HVO fuel at spray velocity of 200 m/s, then, for example, we can see that at the dynamic viscosity value of 1600 μPa the difference of drop size is ~1 μm (25%). At drop velocity of $v2 = 400$ m/s the change of drop size is 0.2 μm (16%).

The dependency between the diameter d_c of the drop leaving the injector and fluid's initial velocity v is given in Fig. 6 and the diameter d_c of the drop leaving the injector and injector's diameter d is given in Fig. 7. Here the density of the gas environment was 17 kg/m^3 and the physical parameters of the fuels correspond to the temperature 90 °C.

Fig. 6 shows that as the drop's velocity increases, the drop's size decreases. Here it is important to point out that the diameter of the injector's opening does not have a significant effect on the drop's size. As the drop's velocity is doubled, its size decreases ~3 times. Physical and chemical properties have an effect on the fuel drop's size. For example, as the fuel's kinematic viscosity increases, the drop size increases (starting from gasoline to FAME or HVO fuel). It is important that no drop size difference is evident in the case of FAME and HVO fuels. This might be caused by the difference between dynamic viscosities and surface tensions. The dynamic viscosity of the FAME fuel is greater than that of the HVO fuel, but the surface tension of HVO is greater
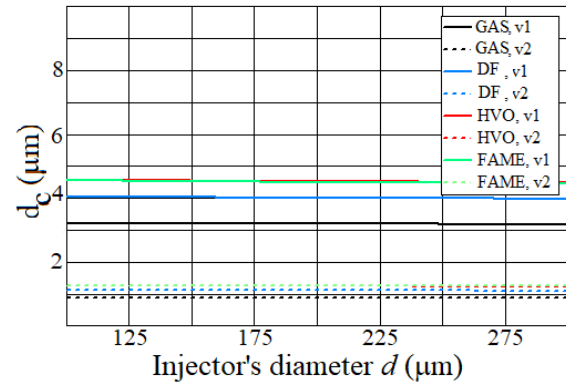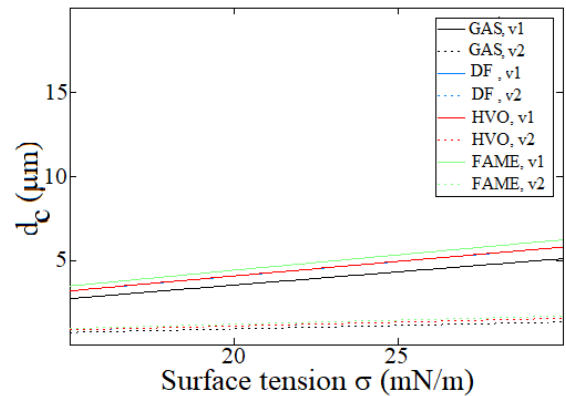

Figure 8: Dependency between diameter dc of the drop leaving the injector and fluid's surface tension σ at two spray velocities v ($v1$ = 200 m/s, $v2$ = 400 m/s). The x-axis value range 15-30 mN/m corresponds to typical surface tensions of fuels at temperatures 90 °C (Table 1).

than that of FAME. Therefore, the change of the drop size is within the same magnitude. Fig. 7 shows that the diameter of the injector's opening does not have a significant effect on drop size in the spray regardless of spray velocity.

Fig. 8 shows the fuel drop size according to the surface tensions of fuels at various spray velocities. The figure shows that as the surface tension increases, the drop size also increases. It is important that the fuel's surface tension has a greater effect on drop size at lower velocities ($v1$ = 200 m/s) than at higher velocities ($v2$ = 400 m/s).

In conclusion, it can be claimed that the fuel drop's size is significantly influenced by the velocity v of the fuel spray, dynamic viscosity μ, density ρ and surface tension factor σ. In order to characterize the drops formed during the preparation of the air-fuel mixture, these parameters must be viewed separately and the physical and chemical properties of each fuel shall be taken into account and projected into the working conditions of a real engine.

The data in Table 3 takes into account that the temperature of the sprayed fuel and the density of the spraying environment are comparable to the actual environment in the en-

Table 3: The calculated values of the Weber numbers *We* (equations (18) and (19)) in the case of the different diameters d_1, d_2 of the colliding drops and impact parameter *B*

	1	2	3	4	5	6
Diameter d_1 (μm)	5	5	5	5	5	5
Diameter d_2 (μm)	5	5	5	10	10	10
Drop size ratio γ	1.0	1.0	1.0	2.0	2.0	2.0
Drop size ratio Δ	1.0	1.0	1.0	0.5	0.5	0.5
Distance b (μm) (Fig. 1)	0	100	400	0	150	600
Impact parameter *B*	0	0.20	0.80	0	0.20	0.80
η_1	1	0.25	-0.95	1.00	0.43	-0.74
η_2	1	0.25	-0.95	0.13	0	-
ξ	0	0.20	0.80	0	0.15	0.60
λ	2	1.60	0.40	1.50	1.20	0.30
φ_1	1	0.90	0.10	0	0.86	0.22
φ_2	1	0.90	0.10	0.84	0.65	0.06
Wereflection (eq. (18))	4.9	19.3	-	30.8	-	-
Westretching (eq. (19))	-	167.8	4.2	38.7	153.4	5.4

gine cylinder. Here, 90 °C was the chosen temperature of the sprayed fuel [122], which corresponds to the temperature of the working engine. The density of the spraying environment was 17 kg/m^3.

6. Mathematical representation of reflexive and stretching separation

The description of the collision of fuel drops is based on the assumption that the drops move confluently and collisions only take place when one fuel drop catches up with another one in the fuel spray. The movement, collision and separation of drops is described in Fig. 9 [123]. The calculations are based on the assumption that after the collision of drops in the fuel spray, reflexive and stretching separation occur.

Reflexive separation occurs in the case of large Weber numbers *We* and low values of impact parameter *B*. This means either frontal impact or a similar situation. If the Weber number is large (<100) and the impact parameter is growing, then stretching separation becomes dominant after the collision of the drops. Impact parameter *B* also determines the number of collisions [124].

In order to describe these two processes, the kinetic energy of two colliding drops and the law of conservation of the surface energy of the temporarily joined drops shall be used. The Weber number for separation of drops for the two processes can be described as follows [123]:

$$We_{\text{reflection}} > \frac{3\left[7\left(1+\Delta^3\right)^{\frac{1}{3}} - 4\left(1+\Delta^2\right)\right]\Delta\left(1+\Delta^3\right)^2}{\Delta^6\eta_1 + \eta_2} \quad (18)$$

which applies to reflexive separation; and

$$We_{\text{stretching}} > \frac{4\left(1+\Delta^3\right)^2\left[3\left(1+\Delta\right)\left(1-B\right)\left(\Delta^3\varphi_1+\varphi_2\right)\right]^{\frac{1}{2}}}{\Delta^2\left[\left(1+\Delta^3\right) - \left(1-B^2\right)\left(\varphi_1+\Delta^3\varphi_2\right)\right]} \quad (19)$$

which applies to stretching separation. The dimensionless constants η_1, η_2 and ξ (Table 3) are used to simplify the calculations and these are obtained as follows:

$$\eta_1 = 2\left(1-\xi\right)^2\left(1-\xi^2\right)^{\frac{1}{2}} - 1 \quad (20)$$

$$\eta_2 = 2\left(\Delta-\xi\right)^2\left(\Delta-\xi^2\right)^{\frac{1}{2}} - \Delta^3 \quad (21)$$

$$\xi = \frac{1}{2}B\left(1+\Delta\right) \quad (22)$$

The dimensionless values of φ_1 and φ_2 are used to describe the stretching separation and these values denote the respective proportions of spatial areas in joined drops. The values of φ_1 and φ_2, parts of interaction volumes V_{1i}, V_{2i} and interaction volume V_i can be represented as follows:

$$\varphi_1 = \begin{cases} 1 - \frac{1}{4^3}\left(2\Delta-\lambda\right)^2\left(\Delta+\lambda\right) \\ \frac{\lambda^2}{4^3}\left(3\Delta-\lambda\right) \end{cases} \quad (23)$$

$$\varphi_2 = \begin{cases} 1 - \frac{1}{4}\left(2-\lambda\right)^2\left(1+\lambda\right) \\ \frac{\lambda^2}{4}\left(3-\lambda\right) \end{cases} \quad (24)$$

$$V_{ji} = \varphi_j V_j \quad (25)$$

$$V_i = V_{1i} + V_{2i} \quad (26)$$

The dimensionless value of λ is expressed as follows:

$$\lambda = \left(1-B\right)\left(1+\Delta\right) \quad (27)$$

The selection criterion for the value of φ_1 is $h > r_1$ and $h < r_1$ respectively and the selection criterion for the value of φ_2 is $h > r_2$ and $h < r_2$ respectively. The value h marks the interaction height and is expressed as follows:

$$h = \frac{1}{2}\left(D_1 + D_2\right)\left(1-B\right) \quad (28)$$

The values of r_1 and r_2 express the radii of drops. In order to understand better the equations (18)-(27), several numeric examples have been given in Table 3.

Situation 1 describes the frontal impact ($B = 0$) of two drops with equal diameters. The Weber number values calculated according to equations 18 and 19 show that if *Wereflection* > 4.9, then reflexing separation takes place with no stretching separation occurring. If none of the separations occur according to the calculations of Table 3, then it must be either bouncing or coalescence of the drops. This model does not discuss these cases further.

If the value of the impact parameter *B* is greater ($B = 0.20$), then it corresponds to a situation in which two drops collide under conditions similar to a frontal impact. In such cases reflexive separation starts to occur from the value *Wereflection* > 19.3 onwards and stretching separation *Westretching* >167.8.

In situation 3 the drops nearly graze each other ($B = 0.80$). Reflexive separation does not occur in this situation. Stretching separation will occur already with smaller Weber numbers (*Westretching* > 4.2).

Situation 4 constitutes a frontal impact of two drops ($B = 0$), whereby one of the drops has twice the diameter of the other one (size ratio of colliding drops is $\gamma = 0.5$). Reflexive separation will occur starting from the value *Wereflection* >30.8 and stretching separation *Westretching* > 38.7. In comparison to situation 1, the greater values of the Weber numbers are caused by the fact that the larger drop swallows the smaller one. In case of lower *We* values; surface tension causes the domination of coalescence.

In situations 5 and 6 the size ratio of colliding drops is still $\gamma = 0.5$, but the impact parameter has been increased to $B = 0.20$ and $B = 0.80$ respectively. Reflexive separation does not occur in any of the situations. In situation 5, stretching separation will start occurring from *Westretching* > 153.4 onwards and in situation 6 *Westretching* > 5.4.

It should be noted that in the case of stretching separation, the interaction height h and interaction volume Vi are much smaller than in the case of reflexive separation. With reflexive separation, the total volume of joined drops is equal to the interaction volume.

The separation volume coefficient C_v is introduced to determine the volume of the fluid separating from two colliding drops and it is defined as the ratio of the volume separating from the two drops and the interaction volume. It is presumed [125] that C_v is equal to the energy needed for separation and the total energy of the two colliding drops:

$$C_v = \frac{\text{KE}_{\text{separation}} - \text{PE}_{\text{coalescence}}}{\text{KE}_{\text{separation}} + \text{PE}_{\text{coalescence}}} \quad (29)$$

KEseparation describes the separation kinetic energy and *PEcoalescence* the surface tension energy which is needed to sustain the coalescence of the two drops. In the case of reflexive separation, the *KEseparation* and *PEcoalescence* can be presented as follows:

$$KE_{\text{separation}} =$$
$$\sigma\pi D_2^2 \left[\left(1 + \Delta^2\right) - \left(1 + \Delta^3\right)^{\frac{2}{3}} + \frac{\text{We}}{12\Delta\left(1+\Delta^3\right)^2}\left(\Delta^6\eta_1 + \eta_2\right) \right] \quad (30)$$

$$\text{PE}_{\text{coalescence}} = 0.75\sigma\pi \left(D_1^3 + D_2^3\right)^{\frac{2}{3}} \quad (31)$$

In the case of stretching separation *KEseparation* and *PEcoalescence* can be presented as follows:

$$KE_{\text{separation}} =$$
$$\tfrac{1}{2}\rho\left(v_1 + v_2\right)^2 V_2 \left\{ \frac{\Delta^3}{\left(1+\Delta^3\right)^2}\left[\left(1 + \Delta^3\right) - \left(1 - B^2\right)\left(\varphi_1 + \Delta^3\varphi_2\right)\right] \right\} \quad (32)$$

$$\text{PE}_{\text{coalescence}} = \sigma \left[2\pi V_2 D_2 \lambda \left(\Delta^3\varphi_1 + \varphi_2\right)\right]^{\frac{1}{2}} \quad (33)$$

V_2 in equations (32) and (33) marks the volume of the second drop before the collision.
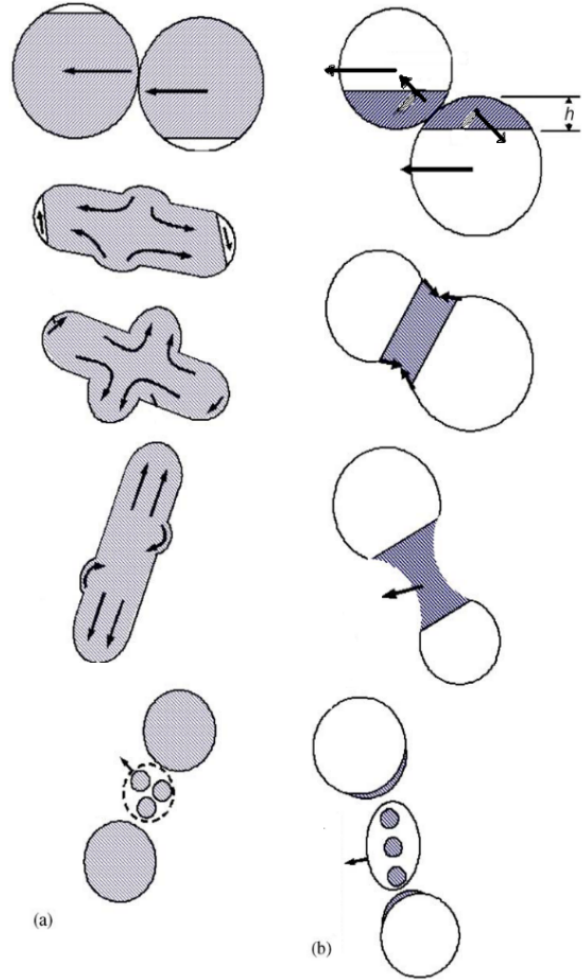

Figure 9: Schematic representation of (*a*) reflexive and (*b*) stretching separation [123]

Taking into account the separation volume coefficient in equation (29) and the values of φ_1 in equation (23) and φ_2 in equation (24), the diameters *dc* of the drops after the collision can be calculated as follows:

$$d_{c1} = (1 - C_v\varphi_1)^{\frac{1}{3}} d_1 \quad (34)$$

$$d_{c2} = (1 - C_v\varphi_2)^{\frac{1}{3}} d_2 \quad (35)$$

where d_1 and d_2 are the respective diameters of the first and second drop before the collision, d_{c1} and d_{c2} are the respective diameters of the first and second drop after the collision.

Fig. 10 shows the relative diameters of drops for different impact parameters. This illustrates the change of size of the drops breaking out and colliding. Calculations have been performed for four fuel types. In the case of the relation $\Delta 1 = 0.5$, the ratio of the sizes of the formed drop and the collided drop changes. This means that with a small impact parameter, the size of the drop formed after the collision is a smaller percentage of the drop size before collision in com-
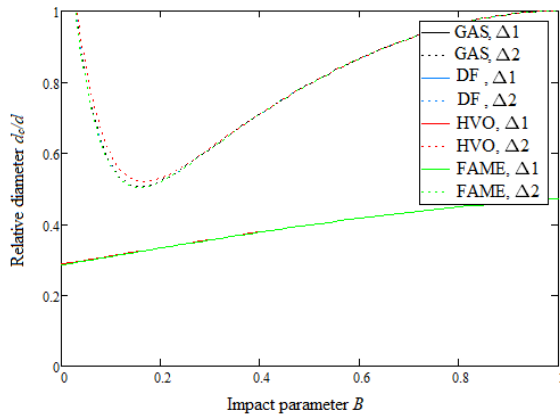
Figure 10: The dependency of the relative diameter d_c/d of a drop that formed after the collision and the impact parameter B at two different colliding drop diameter ratios $\triangle$ (equation 4) ($\triangle 1 = -0.5$, $\triangle 2 = 1.0$) in the case of four different fuel types

parison to the values of greater impact parameters. In simpler terms this means that small values of impact parameter result in smaller drops after the collision than when there are greater values of the impact parameter. It is important feature about the relation of d_c/d for various fuels that the ratio of change of drop size does not change significantly for the value $\triangle 1$. Here we can conclude that the injection of fuels with different physical and chemical properties into the engine cylinder does not result in a significant difference in the quality of the air-fuel mixture.

In a situation where $\triangle 2 = 1$, the influence of the impact parameter on the relative drop diameter in the fuel spray changes significantly. It can be seen from the figure that at the impact parameter's values $B = 0$–0.15 the drop size ratio increases as the impact parameter increases. At the values $B = 0.15 - 1$ the relative diameter of the drops increases as the value of the impact parameter increases. It can be further seen from the graph that at the impact diameter value of $B = 0.22$, the fuel properties have an influence on drop size. For example, at the value of $B = 0.15$ the drop of gasoline after breakout is $\sim 2.5\%$ smaller compared to the HVO fuel. The comparison of FAME fuel and diesel fuel does not reveal a significant change in drop size ratio. The drop size ratio of diesel fuel remains at the same level as gasoline and FAME fuel.

Fig. 10 was obtained with the parameters $v1 = v2 = 200$ m/s and the physical parameters of the fuels correspond to the temperature of 90℃. Fig. 10 shows that drop size can differ in the air-fuel mixture at various values of $\triangle$. It can be concluded that the air-fuel mixture of fuels with high viscosity (for example, HVO) contains somewhat larger drops than the mixture of low viscosity fuel. At the same time, the drops of FAME fuel are in the same magnitude as gasoline and diesel fuel. In addition to viscosity, another important influencing factor is surface tension. At low values of B, the ratio d_c/d is mostly determined by the fuel's surface tension forces. If the value of B is greater, then the interaction vol-

ume remains smaller, which means that the ratio d_c/d is also greater.

Table 4 was prepared to illustrate better the breakout of fuel drops. The table gives the drop sizes of various fuels at various values of the impact parameter B. Table 4 exemplifies also a situation in which the colliding drops are equal. The physical parameters of fuels in Table 4 correspond to the temperature of 90℃. In the first case (1), the value of C_v is negative for stretching separation, which means that stretching separation does not occur. The positive value of C_v shows that reflexive separation takes place.

In the other cases (2-4) reflexive and stretching separation of drops occur. The main difference between the different cases is that when the impact parameter's value is $B = 0.1$, then the drop size of diesel fuel and gasoline is $\sim 5\%$ smaller than that of HVO and FAME fuels. It can be deduced from here that the drop size in the air-fuel mixture of HVO and FAME fuels is somewhat greater than that of diesel fuel. Here the air-fuel mixture corresponds to general knowledge, according to which the drop size in air-fuel mixtures of high viscosity fuels is greater. At the same time, it is not clear why the soot level in emission gas of biofuels is lower. If we presume that the use of FAME fuels results in lower soot levels in the exhaust gas mostly due to the oxygen content in the fuel, then what is the reason for the lower soot level of HVO fuel? In conclusion, it can be claimed that the drop size of biofuels in air-fuel mixture is somewhat larger. The approach of this article does not give the answer why the soot level in the engine's emission gas decreases when HVO and FAME fuels are used. At the same time, the results illustrate that there are no important differences in the quality of air-fuel mixture. In order to account for the reduced soot level, it is necessary to study experimentally the breakout of drops in the fuel spray, the effect of oxygen content on the combustion of fuel and the effect of various fuel fractions on the combustion process.

7. Summary

We investigated the physical parameters of four different types of fuels (gasoline, diesel fuel, HVO, FAME) and phenomena related to these parameters, which include the spraying of fuel drops and the coalescence and collision of these drops. The fuel drop sizes after leaving the injector and after mutual collisions were calculated.

The results can be summarized as follows:

1. In the hybrid breakout model, spray velocity has a significant effect on drop size. As the spray velocity increases, drop size in the fuel spray decreases. When considering the conditions under which fuel is sprayed in a working engine, viscosity and surface tension are factors that have a significant effect mostly at low spraying velocities. The higher the velocity of fuel spray, the lower the effect that viscosity and surface tension have on drop size in the fuel spray. According to the model used, the diameter of the injection opening does not have an effect on drop size in the fuel spray.

Table 4: Drop diameter d_c after collision and the value of separation coefficient Cv in the case of collision of two drops of equal diameter.

Diameter d_1 (μm)	5.0	5.0	5.0	5.0
Diameter d_2 (μm)	5.0	5.0	5.0	5.0
Velocity v1 (m/s)	100	100	100	100
Velocity v2 (m/s)	100	100	100	100
Impact parameter B	0	0.10	0.20	0.80
Interaction volume to volume ratio V_i/V	1.00	0.97	0.90	0.10
Gasoline (GAS)	Gasoline (GAS)	Gasoline (GAS)	Gasoline (GAS)	Gasoline (GAS)
Weber number We	7878	7878	7878	7878
Separation volume coefficient C_v (eq (29)) (reflexing)	0.99	0.99	0.99	1.00
Separation volume coefficient C_v (eq (29)) (stretching)	-1.00	0.84	0.96	1.00
Drop size dc after separation (μm)	5.0	2.8	2.6	4.8
Diesel Fuel (DF)	Diesel Fuel (DF)	Diesel Fuel (DF)	Diesel Fuel (DF)	Diesel Fuel (DF)
Weber number We	9111	9111	9111	9111
Separation volume coefficient C_v (eq (29)) (reflexing)	0.99	0.99	0.99	1.00
Separation volume coefficient C_v (eq (29)) (stretching)	-1.00	0.86	0.96	1.00
Drop size dc after separation (μm)	5.0	2.7	2.6	4.8
HVO	HVO	HVO	HVO	HVO
Weber number We	4762	4762	4762	4762
Separation volume coefficient C_v (eq (29)) (reflexing)	0.99	0.99	0.99	1.00
Separation volume coefficient C_v (eq (29)) (stretching)	-1.00	0.75	0.93	1.00
Drop size dc after separation (μm)	5.0	3.2	2.7	4.8
FAME	FAME	FAME	FAME	FAME
Weber number We	5780	5780	5780	5780
Separation volume coefficient C_v (eq (29)) (reflexing)	0.99	0.99	0.99	1.00
Separation volume coefficient C_v (eq (29)) (stretching)	-1.00	0.79	0.94	1.00
Drop size dc after separation (μm)	5.0	3.1	2.7	4.8

2. When biodiesel fuel is used, according to the hybrid breakout model drop size in the fuel spray is somewhat greater (~12%). As the fuel spray velocity increases, the size ratio of drop increases.

3. When drops collide in the fuel spray, generally the drop size increases as the value of impact parameter B increases if the drop size ratio of colliding drops is $\Delta = 0.5$. If the drop size ratio of colliding drops is $\Delta = 1$, then at the impact parameter's value of $B = 0.1$, the size of drops after breakout is the smallest. As impact parameter B increases or decreases, drop size in the fuel spray starts to increase. The physical and chemical properties of fuels do not have a significant effect on drop size. Minor differences occur when drops of the same size collide at the impact parameter value range of $B = 0.5..1.5$.

4. The biodiesel air-fuel mixture contains somewhat larger drops than the air-fuel mixture of diesel fuel. The results show that the model used in the study cannot be used to account for the reduction in the soot level of biodiesel fuel. This is due to the fact that the quality of the biodiesel air-fuel mixture is not significantly different from diesel fuel.

There are several further questions that need to be addressed:

1. How does the oxygen contained in the fuel influence the soot level of the combustion of the fuel?

2. How do the fuel drop sizes change in the injection chamber for the four types of fuel (gasoline, diesel fuel, HVO, FAME) both temporally and spatially?

The topic of this article is related to the scope of the Journal of the Power and Technologies by the theme of renewable energy. The article provides an overview of the behavior of biofuel drops in fuel spray and supplements the knowledge base of the journal with explanations of issues relating to sprays of biofuels.

References

[1] A. Kuut, R. Ilves, K. Kuut, V. Raide, K. Ritslaid, J. Olt, Influence of European Union Directives on the Use of Liquid Biofuel in the Transport Sector, Procedia Engineering (2017) 30–39.

[2] J. Xue, T. E. Grift, A. C. Hansen, Effect of biodiesel on engine performances and emissions, Renewable and Sustainable Energy Reviews 15 (2011) 1098–1116.

[3] H. Hazar, Effects of biodiesel on a low heat loss diesel engine, Renewable Energy 34 (2009) 1533–1537.

[4] A. N. Ozsezen, M. Canakci, A. Turkcan, C. Sayin, Performance and combustion characteristics of a DI diesel engine fueled with waste palm oil and canola oil methyl esters, Fuel 88 (2009) 629–636.

[5] Z. Utlu, M. S. Koçak, The effect of biodiesel fuel obtained from waste frying oil on direct injection diesel engine performance and exhaust emissions, Renewable Energy 33 (2008) 1936–1941.

[6] H. Ozgunay, S. Çolak, G. Zengin, O. Sari, H. Sarikahya, L. Yuceer, Performance and emission study of biodiesel from leather industry pre-fleshings, Waste Management 27 (2007) 1897–1901.

[7] C. Kaplan, R. Arslan, A. Surmen, Performance characteristics of sunflower methyl esters as biodiesel, Energy Sources Part A Recovery Utilization and Environmental Effects 28 (2006) 751–755.

[8] J. F. Reyes, M. A. Sepúlveda, PM-10 emissions and power of a diesel engine fueled with crude and refined biodiesel from salmon oil, Fuel 85 (2006) 1714–1719.

[9] H. Raheman, A. G. Phadatare, Diesel engine emissions and performance from blends of karanja methyl ester and diesel, Biomass and Bioenergy 27 (2004) 393–397.

[10] Y. Ulusoy, Y. Tekin, M. Cetinkaya, F. Karaosmanoglu, The engine tests of biodiesel from used frying oil, Energy Sources 26 (2004) 927–932.

[11] S.-H. Choi, Y. Oh, The emission effects by the use of biodiesel fuel, International Journal of Modern Physics B 20 (2006) 4481–4486.

[12] B.-F. Lin, J.-H. Huang, D.-Y. Huan, Experimental study of the effects of vegetable oil methyl ester on DI diesel engine performance characteristics and pollutant emissions, Fuel 88 (2009) 1779–1785.

[13] D. H. Qi, L. M. Geng, H. Chen, Y. Z. H. Bian, J. Liu, X. C. H. Ren, Combustion and performance evaluation of a diesel engine fueled

with biodiesel produced from soybean crude oil, Renewable Energy 34 (2009) 2706–2713.

[14] M. Lapuerta, J. M. Herreros, L. L. Lyons, R. García-Contreras, Y. Briceño, Effect of the alcohol type used in the production of waste cooking oil biodiesel on diesel performance and emissions, Fuel 87 (2008) 3161–3169.

[15] H. Kim, B. Choi, The effect of biodiesel and bioethanol blended diesel fuel on nanoparticles and exhaust emissions from CRDI diesel engine, Renewable Energy 35 (2010) 157–163.

[16] X. Meng, G. Chen, Y. Wang, Biodiesel production from waste cooking oil via alkali catalyst and its engine test, Fuel Processing Technology 89 (2008) 851–857.

[17] A. Hull, I. Golubkov, B. Kronberg, J. van Stam, Alternative fuel for a standard diesel engine, International Journal of Engine Research 7 (2006) 51–63.

[18] M. Gumus, S. Kasifoglu, Performance and emission evaluation of a compression ignition engine using a biodiesel (apricot seed kernel oil methyl ester) and its blends with diesel fuel, Biomass and Bioenergy 34 (2010) 134–139.

[19] A. Pal, A. Verma, S. S. Kachhwaha, S. Maji, Biodiesel production through hydrodynamic cavitation and performance testing, Renewable Energy 35 (2010) 619–624.

[20] A. S. Ramadhas, C. Muraleedharan, S. Jayaraj, Performance and emission evaluation of a diesel engine fueled with methyl esters of rubber seed oil, Renewable Energy 30 (2005) 1789–1800.

[21] D. Sharma, S. L. Soni, J. Mathur, Emission reduction in a direct injection diesel engine fueled by neem-diesel blend, Energy Reports 31 (2009) 500–508.

[22] M. Guru, A. Koca, O. Can, C. Çınar, F. Şahin, Biodiesel production from waste chicken fat based sources and evaluation with Mg based additive in a diesel engine, Renewable Energy 35 (2010) 637–643.

[23] L. Zhu, W. Zhang, W. Liu, Z. Hunag, Experimental study on particulate and NOx emissions of a diesel engine fueled with ultra low sulfur diesel, RME-diesel blends and PME-diesel blends, Science of Total Environment 408 (2010) 1050–1058.

[24] K. Ryu, The characteristics of performance and exhaust emissions of a diesel engine using a biodiesel with antioxidants, Bioresource Technology 101 (2010) S78–S82.

[25] J. M. Luján, V. Bermúdez, B. Tormos, B. Pla, Comparative analysis of a DI diesel engine fuelled with biodiesel blends during the European MVEG-A cycle: Performance and emissions (II), Biomass and Bioenergy 33 (2009) 948–956.

[26] C. S. Cheung, L. Zhu, Z. Huang, Regulated and unregulated emissions from a diesel engine fueled with biodiesel and biodiesel blended with methanol, Atmospheric Environment 43 (2009) 4865–4872.

[27] S. J. Deshmukh, L. B. Bhuyar, Transesterified Hingan (Balanites) oil as a fuel for compression ignition engines, Biomass and Bioenergy 33 (2009) 108–112.

[28] A. Tsolakis, A. Megaritis, M. L. Wyszynski, K. Theinnoi, Engine performance and emissions of a diesel engine operating on diesel-RME (rapeseed methyl ester) blends with EGR (exhaust gas recirculation), Energy 32 (2007) 2072–2080.

[29] H. Raheman, S. V. Ghadge, Performance of compression ignition engine with mahua (Madhuca indica) biodiesel, Fuel 86 (2007) 2568–2573.

[30] D. Agarwal, S. Sinha, A. K. Agarwal, Experimental investigation of control of NOx emissions in biodiesel-fueled compression ignition engine, Renewable Energy 31 (2006) 2356–2369.

[31] S. Puhan, N. Vedaraman, V. B. R. Boppana, J. Jeychandran, G. Sankarnarayanan, Mahua oil (Madhuca Indica seed oil) methyl ester as biodiesel-preparation and emissioon characterstics, Biomass and Bioenergy 28 (2005) 87–93.

[32] M. Canakci, Performance and emissions characteristics of biodiesel from soybean oil, Proceedings of the Institution of Mechanical Engineers, Part D: Journal of Automobile Engineering 219 (2005) 915–922.

[33] M. Canakci, J. H. van Gerpen, Comparison of engine performance and emissions for petroleum diesel fuel, yellow grease biodiesel, and soybean oil biodiesel, Transactions of the ASAE 46 (2003) 937–944.

[34] A. Senatore, M. Cardone, V. Rocco, M. V. Prati, A Comparative Analysis of Combustion Process in D.I. Diesel Engine Fueled with Biodiesel

[35] M. J. Haas, K. M. Wagner, T. L. Alleman, R. L. McCormick, Engine performance of biodiesel fuel prepared from soybean soapstock: a high quality renewable fuel produced from a waste feedstock, Energy & Fuels 15 (2001) 1207–1212.

[36] P. K. Sahoo, L. M. Das, M. K. G. Babu, S. N. Naik, Biodiesel development from high acid value polanga seed oil and performance evaluation in a CI engine, Fuel 86 (2007) 448–454.

[37] B. Baiju, M. K. Naik, L. M. Das, A comparative evaluation of compression ignition engine characteristics using methyl and ethyl esters of Karanja oil, Renewable Energy 34 (2009) 1616–1621.

[38] F. Wu, J. Wang, W. Chen, S. Shuai, A study on emission performance of a diesel engine fueled with five typical methyl ester biodiesels, Atmospheric Environment 43 (2009) 1481–1485.

[39] Y. Ulusoy, R. Arslan, C. Kaplan, Emission characteristics of sunflower oil methyl ester, Energy Sources Part A 11 (2009) 906–910.

[40] C.-Y. Lin, R.-J. Li, Engine performance and emission characteristics of marine fish-oil biodiesel produced from the discarded parts of marine fish, Fuel Processing Technology 90 (2009) 883–888.

[41] D. Tziourtzioumis, L. Demetriades, O. Zogou, T. Stamatelos, Experimental investigation of the effect of a B70 biodiesel blend on a common-rail passenger car diesel engine, Proceedings of the Institution of Mechanical Engineers Part D Journal of Automobile Engineering 223 (2009) 685–701.

[42] M. Zheng, M. C. Mulenga, G. T. Reader, M. Wang, D. S.-K. Ting, J. Tjong, Biodiesel engine performance and emissions in low temperature combustion, Fuel 87 (2008) 714–722.

[43] M. E. Tat, J. H. van Gerpen, P. S. Wang, Fuel Property Effects on Injection Timing, Ignition Timing and Oxides of Nitrogen Emissions from Biodiesel-Fueled Engines, Transactions ASABE 50 (2007) 1123–1128.

[44] S. Kalligeros, F. Zannikos, S. Stournas, E. Lois, G. Anastopoulus, C. Teas, F. Sakellaropoulos, An investigation of using biodiesel/marine diesel blends on the performance of a stationary diesel engine, Biomass and Bioenergy 24 (2003) 141–149.

[45] M. Lapuerta, O. Armas, R. Ballestros, Diesel particulate emissions from biofuels derived from Spanish vegetable oils, SAE Paper 2002 1 (2002) 1657.

[46] H. Jung, D. B. Kittelson, M. R. Zachariah, Characteristics of SME biodiesel-fueled diesel particle emissions and the kinetics of oxidation, Environmental Science Technologies 40 (2006) 4949–4955.

[47] A. Monyem, J. H. van Gerpen, The effect of biodiesel oxidation on engine performance and emissions, Biomass and Bioenergy 20 (2001) 317–325.

[48] M. S. Graboski, R. L. McCormick, T. L. Alleman, A. M. Herring, The effect of biodiesel composition on engine emissions from a DDC series 60 diesel engine, National Renewable Energy Laboratory (2003) NREL/SR–510–31461.

[49] W. G. Wang, D. W. Lyons, N. N. Clark, M. Gautam, Emissions from nine heavy trucks fuelled by diesel and biodiesel blend without engine modification, Environmental Science and Technology 34.

[50] M. Cardone, M. V. Prati, V. Rocco, M. Seggiani, A. Senatore, S. Vitolo, Brassica carinata as an alternative oil crop for the production of biodiesel in italy engine performance and regulated and unregulated exhaust emissions, Environmental Science & Technology 36 (2002) 4656–4662.

[51] N. Y. Kado, P. A. Kuzmicky, Progress in Energy and Combustion Science, National Renewable Energy Laboratory (2003) NREL/SR–510–31463.

[52] M. Lapuerta, O. Armas, R. Ballestros, M. Carmona, Fuel formulation effects on passenger car diesel engine particulate emissions and composition, SAE Paper 2000 (2000) 1850.

[53] O. Armas, J. J. Hernández, M. D. Cárdenas, Reduction of diesel smoke opacity from vegetable oil methyl esters during transient operation, Fuel 85 (2006) 2427–2438.

[54] K. Yamane, A. Ueta, Y. Shimamoto, Influence of physical and chemical properties of biodiesel fuels on injection, combustin and exhaust emission characteristics in a direct injection compression ignition engine, International Journal of Engine Research 2 (2001) 249–261.

[55] M. Lapuerta, O. Armas, J. M. Herreros, Emissions from a diesel-biodiesel blend in an automotive diesel engine, Fuel 1 (2008) 25–31.

[56] M. Lapuerta, O. Armas, R. Ballesteros, J. Fernández, Diesel emissions from biofuels derived from Spanish potential vegetable oils, Fuel 84 (2005) 773–780.

[57] K. Dincer, Lower Emissions from Biodiesel Combustion, Energy Sources 30 (2008) 963–968.

[58] G. Fontaras, G. Karavalakis, M. Kousoulidou, T. Tzamkiozis, L. Ntziachristos, E. Bakeas, S. Stournas, Z. Samaras, Effects of biodiesel on passenger car fuel consumption, regulated and non-regulated pollutant emissions over legislated and real-world driving cycles, Fuel 88 (1608-1617) 2009.

[59] T. Bohl, A. Smallbone, G. Tian, A. P. Roskilly, Particulate number and NOx trade-off comparisons between HVO and mineral diesel in HD applications, Fuel 215 (2018) 90–101.

[60] C. Vo, C. Charoenphonphanich, P. Karin, S. Susumu, K. Hidenori, Effects of variable O2 concentrations and injection pressures on the combustion and emissions characteristics of the petro-diesel and hydrotreated vegetable oil-based fuels under the simulated diesel engine condition, Journal of the Energy Institute 91 (2018) 1071–1084.

[61] G. Brenn, Droplet collision. Handbook of atomization and sprays: theory and applications, Nasser Ashgriz, 2011.

[62] N. Nikolopoulos, K.-S. Nikas, G. Bergeles, A numerical investigation of central binary collision of droplets, Computers & Fluids 38 (2009) 1191–1202.

[63] M. R. H. Nobari, J. Jan, G. Tryggvason, Head-on collision of drops - a numerical investigation, Physics of Fluids 8 (1995) 29–42.

[64] J. Li, Macroscopic Model for Head-On Binary Droplet Collisions in a Gaseous Medium, Physics Review Letters 117.

[65] M. Liu, D. Bothe, Numerical study of head-on droplet collisions at high Weber numbers, Journal of Fluid Mechanics 789 (2016) 785–805.

[66] J. Qian, C. K. Law, Regimes of coalescence and separation in droplet collision, Journal of Fluid Mechanics 331 (1997) 59–80.

[67] R. S. Volkov, G. V. Kuznetsov, P. A. Strizhak, Statistical analysis of consequences of collisions between two water droplets upon their motion in a high-temperature gas flow, Technical Physics Letters 41 (2015) 840–843.

[68] D. V. Antonov, R. S. Volkov, G. V. Kuznetsov, P. A. Strizhak, Experimental Study of the Effects of Collision of Water Droplets in a Flow of High-Temperature Gases, Journal of Engineering Physics and Thermophysics 89 (2016) 100–111.

[69] R. D. Reitz, F. V. Bracco, Mechanisms of Breakup of Round Liquid Jets, The Encyclopedia of Fluid Mechanics 3 (1986) 223–249.

[70] R. D. Reitz, Modeling atomization processes in high-pressure vaporizing sprays, Atomisation and Spray Technology 3 (1987) 309–337.

[71] P. O'Rourke, A. Amsden, The Tab Method for Numerical Calculation of Spray Droplet Breakup, SAE Technical Paper 872089.

[72] Diesel-Egnine Management, 4th Edition, Robert Bosch GmbH, 2006.

[73] S. Budavari, The Merck index : an encyclopedia of chemicals, drugs, and biologicals, Whitehouse Station, N.J Merck, 2001.

[74] X. Jiang, A. J. James, Head-on collision of two equal-sized drops with van der Waals forces, Advances in Fluid Mechanics 37.

[75] M. Saroka, N. Ashgriz, M. Movassat, Numerical Investigation of Head-on Binary Drop Collisions in a Dynamically Inert Environment, Journal of Applied Fluid Mechanics 5 (2012) 23–37.

[76] K. G. Krishnan, E. Loth, Effects of gas and droplet characteristics on drop-drop collision outcome regimes, International Journal of Multiphase Flow 77 (2015) 171–186.

[77] Y. R. Zhang, X. Z. Jiang, K. H. Luo, Bounce regime of droplet collisions: A molecular dynamics study, Journal of Computational Science 17 (2016) 457–462.

[78] J.-P. Estrade, H. Carentz, G. Lavergne, Y. Biscos, Experimental investigation of dynamic binary collision of ethanol droplets – a model for droplet coalescence and bouncing, International Journal of Heat and Fluid Flow 20 (1999) 486–491.

[79] M. Ashna, M. H. Rahimian, LMB simulation of head-on collision of evaporating and burning droplets in coalescence regime, International Journal of Heat and Mass Transfer 109 (2017) 520–536.

[80] C. Focke, M. Kuschel, M. Sommerfeld, D. Bothe, Collision between high and low viscosity droplets: Direct Numerical Simulations and experiments, International Journal of Multiphase Flow 56 (2013) 81–92.

[81] S. Kim, D. J. Lee, C. S. Lee, Modeling of binary droplet collisions for application to inter-impingement sprays, International Journal of Multiphase Flow 35 (2009) 533–549.

[82] L. F. R. S. Rayleigh, On the instability of jets, London Mathematical Society.

[83] A. M. Worthington, A Study of Splashes, Longmans, 1908.

[84] A. Munnanur, R. D. Reitz, A new predictive model for fragmenting and non-fragmenting binary droplet collisions, International Journal of Multiphase Flow 33 (2007) 873–896.

[85] S. L. Post, J. Abraham, Modeling the outcome of drop–drop collisions in Diesel sprays, International Journal of Multiphase Flow 28 (2002) 997–1019.

[86] F. V. Bracco, Modeling of engine sprays, SAE Transactions 94 (1985) 144–167.

[87] D. L. Siebers, Liquid-phase fuel penetration in Diesel sprays, SAE Technical Paper 980809.

[88] H. Liu, Science and Engineering of Droplets, William Andrew Inc., 1999.

[89] S. Hou, D. P. Schmidt, Adaptive collision meshing and satellite droplet formation in spray simulations, International Journal of Multiphase Flow 32 (2006) 935–956.

[90] H. Hiroyasu, M. Arai, Structures of Fuel Sprays in Diesel Engines, SAE Technical Paper 900475.

[91] H. Hiroyasu, M. Arai, M. Tabata, Empirical Equations for the Sauter Mean Diameter of a Diesel Spray, SAE Technical Paper 890464.

[92] H. Hiruyasu, T. Kadota, Fuel Droplet Size Distribution in Diesel Combustion Chamber, SAE Technical Paper 740715.

[93] P. J. O'Rourke, Collective drop effects on vaporizing liquid sprays, Ph.D thesis, Mechanical and Aerospace Engineering, Princeton University, USA.

[94] Y. Maruyama, T. Chiba, M. Saito, M. Arai, Effect of the inter-impingement system, Proceedings of ILASS-Asia (2001) 241–246.

[95] C. Arcoumanis, M. Gavaises, B. French, Effect of Fuel Injection Processes on the Structure of Diesel Sprays, SAE Technical Paper 970799.

[96] L. Martinelli, F. V. Bracco, R. D. Reitz, Comparisons of computed and measured dense spray jets, Progress in Astronautics and Aeronautics 95 (1984) 484–512.

[97] D. R. Guilenbecher, C. López-Rivera, P. E. Sojka, Secondary atomization, Experiments in Fluids 46 (2009) 371–402.

[98] T. Kekesi, G. Amberg, L. P. Wittberg, Drop deformation and breakup, International Journal of Multiphase Flow 66 (2014) 1–10.

[99] G. Strotos, I. Malgarinos, N. Nikolopoulus, M. Gavaises, Predicting droplet deformation and breakup for moderate Weber numbers, International Journal of Multiphase Flow 85 (2016) 96–109.

[100] F. Xiao, Z. G. Wang, M. B. Sun, N. Liu, X. Yang, Simulation of drop deformation and breakup in supersonic flow, Proceedings of the Combustion Institute 36 (2017) 2417–2424.

[101] G. Strotos, I. Malgarinos, N. Nikolopoulus, M. Gavaises, Aerodynamic breakup of an n-decane droplet in a high temperature gas environment, Fuel 185 (2016) 370–380.

[102] K.-S. Im, K.-C. Lin, M.-C. Lai, M. S. Chon, Breakup modeling of a liquid jet in cross flow, International Journal of Automotive Technology 12 (2011) 489–496.

[103] M. Patterson, R. D. Reitz, Modeling the Effects of Fuel Spray Characteristics on Diesel Engine Combustion and Emission, SAE Technical Paper 980131.

[104] L. Ricart, J. Xin, G. Bower, R. D. Reitz, In-Cylinder Measurement and Modeling of Liquid Fuel Spray Penetration in a Heavy-Duty Diesel Engine, SAE Technical Paper 971591.

[105] J. C. Beale, R. D. Reitz, Modeling spray atomization with the Kelvin-Helmholtz/Rayleigh-Taylor hybrid model, Atomization and Sprays 9 (1999) 623–650.

[106] M. Marek, The double-mass model of drop deformation and secondary breakup, Applied Mathematical Modelling 37 (2013) 7919–7939.

[107] M. Pilch, C. A. Erdman, Use of breakup time data and velocity history data to predict the maximum size of stable fragments for acceleration-induced breakup of a liquid drop, International Journal of Multiphase Flow 13 (1987) 741–757.

[108] G. I. Taylor, The shape and acceleration of a drop in a high-speed air stream, The Scientific Papers by G. I. Taylor 3 (1963) 457–464.

[109] J. A. Nicholls, A. A. Ranger, Aerodynamic shattering of liquid drops, Journal of American Institute of Aeronautics and Astronautics 7 (1969) 285–290.

[110] E. A. Ibrahim, H. Q. Yang, A. J. Przekwas, Modeling of spray droplets deformation and breakup, Journal of American Institute of Aeronautics and Astronautics 9 (1993) 652–654.

[111] S. Som, D. E. Longman, A. I. Ramírez, S. K. Aggarwal, A comparison of injector flow and spray characteristics of biodiesel with petrodiesel, Fuel 89 (2010) 4014–4024.

[112] L. Bravo, C.-B. Kweon, A Review on Liquid Spray Models for Diesel Engine Computational Analysis, Tech. rep. (2014).

[113] A. B. Liu, D. Mather, R. D. Reitz, Modeling the Effects of Drop Drag and Breakup on Fuel Sprays, SAE Technical Paper 930072.

[114] D. M. Gonzalez, Z. Lian, R. D. Reitz, Modeling Diesel Engine Spray Vaporization and Combustion, SAE Technical Paper 920579.

[115] A. B. Chhetri, K. C. Watts, Surface tensions of petro-diesel, canola, jatropha and soapnut biodiesel fuels at elevated temperatures and pressures, Fuel 104 (2013) 704–710.

[116] B. Kegl, L. Lešnik, Modeling of macroscopic mineral diesel and biodiesel spray characteristics, Fuel 222 (2018) 810–820.

[117] F. Wang, J. Wu, Z. Liu, Surface Tensions of Mixtures of Diesel Oil or Gasoline and Dimethoxymethane, Dimethyl Carbonate, or Ethanol, Energy Fuels 20 (2006) 2471–2474.

[118] T. Bohl, G. Tian, A. Smallbone, A. P. Roskilly, Macroscopic spray characteristics of next-generation bio-derived diesel fuels in comparison to mineral diesel, Applied Energy 186 (2017) 562–573.

[119] E. A. Melo-Espinosa, Y. Sánchez-Borroto, M. Errasti, R. Piloto-Rodrígueza, R. Sierens, J. Roger-Riba, A. Christopher-Hansen, Surface Tension Prediction of Vegetable Oils Using Artificial Neural Networks and Multiple Linear Regression, Energy Procedia 57 (2014) 886–895.

[120] Z. Feng, C. Zhan, C. Tang, K. Yang, Z. Huang, Experimental investigation on spray and atomization characteristics of diesel/gasoline/ethanol blends in high pressure common rail injection system, Energy 112 (2016) 549–561.

[121] S. N. Sahasrabudhe, V. Rodriquez-Martinez, M. O'Meara, B. E. Farkas, Density, viscosity, and surface tension of five vegetable oils at elevated temperatures: Measurement and modeling, International Journal of Food Properties 20 (2017) 1965–1981.

[122] W. Zhao, L. Fan, Q. Dong, X. Ma, Study of Fuel Temperature Dynamic Characteristics for Diesel Engine Combination Electronic Unit Pump, Journal of Marine Science and Technology 25 (2017) 220–229.

[123] N. Ashgriz, J. Y. Poo, Coalescence and separation in binary collisions of liquid drops, Journal of Fluid Mechanics 221 (1990) 183–204.

[124] O. O. Taskiran, M. Ergeneman, Trajectory based droplet collision model for spray modeling, Fuel 115 (2014) 896–900.

[125] G. H. Ko, H. S. Ryou, Droplet collision processes in an inter-spray impingement system, Journal of Aerosol Science 36 (2005) 1300–1321.